Open access • Journal Article • DOI:10.1021/NL203325S

Nanoscale Plasmonic Interferometers for Multispectral, High-Throughput Biochemical Sensing — Source link

Jing Feng, Siu Vince, Alec Roelke, Vihang Mehta ...+3 more authors

Institutions: Brown University

Published on: 09 Jan 2012 - Nano Letters (American Chemical Society)

Topics: Interferometry

Plasmon interferometers for high-throughput sensing

Ozlem Yavas and Coskun Kocabas*

Department of Physics, Bilkent University, Ankara 06800, Turkey
**Corresponding author: ckocabas@fen.bilkent.edu.tr*

Received March 16, 2012; revised May 26, 2012; accepted July 6, 2012;
posted July 9, 2012 (Doc. ID 164899); published August 8, 2012

In this letter, we demonstrate a refractive index sensor based on a subwavelength plasmon interferometer. Illumination of an atilt subwavelength slit-grove pair on a metal surface with monochromatic light generates high-contrast interference fringes of the transmitted light. Detection of the refractive index of the dielectric medium on the metal surface is based on examining the relative position of the interference fringes. Integration of the plasmon interferometer with a microfluidic channel provides a sensitive, high-throughput sensor with small detection volume.

OCIS codes: 240.6680, 280.1415, 280.3420.

Small detection volume [1], increased analysis speed, and reduced cost [2] are the main driving forces for miniaturized lab-on-a-chip systems [3]. Subwavelength holes on opaque metal films provide a unique configuration for miniaturized sensors. Transmitted light through these tiny holes is governed by the electronic resonance in the surface of the metal film. Excitation of surface plasmon-polaritons (SPPs) on the metaldielectric interface characterizes the resonance condition. The sensitive dependence of the plasmon resonance condition on the dielectric constant of the medium is used for label-free sensing applications [4].

Surface plasmon resonance (SPR) sensors are widely used to measure biomolecular interactions on functionalized metal surfaces [5–7]. SPPs are confined electromagnetic modes at an interface between two media with opposite permittivity at the working wavelength, that is, a metal—dielectric interface. Gold, silver, and aluminum have negative dielectric constants at the visible spectrum; therefore, they are used as a metal substrates to support SPPs. Variation of the dielectric constant of the medium on the metal layer changes the wavevector of SPPs, which results in a change in the excitation efficiency. Detecting the reflected power from the metal surface through a prism provides a sensitive means of detecting index of refraction. Surface-specific detection together with high sensitivity allows the widespread acceptance of SPR sensors. Different types of SPR sensors have been proposed to increase the detection sensitivity [8,9]. Sensing schemes based on long-range surface plasmons (SPs) [10], localized SPs [11], and transmission through nanohole arrays are examples for sensitive ones. Signal interrogation techniques give another degree of freedom to optimize SPR sensors. Various physical parameters, such as intensity, wavelength [12], and phase [13], have been implemented with different interferometer geometries to improve the detection sensitivity. Recently, subwavelength plasmon interferometers [14,15] have received attention due to their small detection volume and high sensitivity. Different combinations of parallel grooves and slits generate spectral interference in the transmitted light [16]. Measuring the spectrum of the transmitted light provides sensitive methods for label-free sensing [17]. Due to the requirement of a tunable light source or a spectrometer, multispectral plasmon sensors are not very practical for high-throughput applications.

In this letter, we demonstrate a refractive index sensor based on a subwavelength plasmon interferometer using monochromatic light. The main motivation of this work is to introduce a fringe pattern interrogation technique for SP sensors. A very-high-contrast fringe pattern is generated by the plasmon interferometer that consists of a subwavelength slit-groove pair with a small angle between them. The small angle between the groove and the slit provides spatially varying slit-groove distance, which generates a high-contrast interference pattern. By interrogating the relative position of interference fringes, one can determine the refractive index of the dielectric medium on the metal surface. This is a practical yet very sensitive refractive index measurement scheme. The developed subwavelength plasmon interferometer has four distinct advantages: (1) the interferometer uses monochromatic light, (2) the sensor does not need a bulky prism or grating structures to excite SPPs, (3) the signal interrogation requires a simple image processing, and (4) the sensor has very small detection volume (~100 fL).

Figure 1 shows the schematic drawing of the plasmon interferometer. The interferometer consists of a subwavelength slit-groove pair with a small angle between them. The distance between the slit and the groove varies with the position x along the slit, as $d(x) = x \sin \theta$, where θ is the tilt angle. Similar structures were fabricated with the tilt angle (θ) of 5°, 10°, or 15°. Scanning electron microscope (SEM) images of the fabricated slit-groove pairs with tilt angles of 5° and 15° are given in Fig. 1(b) and Fig. 1(c), respectively. The slit-groove pairs are etched using focused Ga^+ ions on 150 nm thick gold film deposited on a quartz substrate. We observed that to obtain high-contrast fringes, the metal film should be thicker than 100 nm. The length of the slit and groove are 50 μm. The width of the slit and the groove are 100 nm and 200 nm, respectively. The widths of the groove and the slit determine the contrast of the interference pattern. The slit extends through the gold layer, and the groove has a depth of 100 nm.

To obtain the interference patterns, we illuminated the slit-groove pairs with a collimated diode laser ($\lambda = 635$ nm). The polarization of the laser was orthogonal to the slit length. The transmitted light was imaged by a CCD camera (Scion Corp.) through a microscope

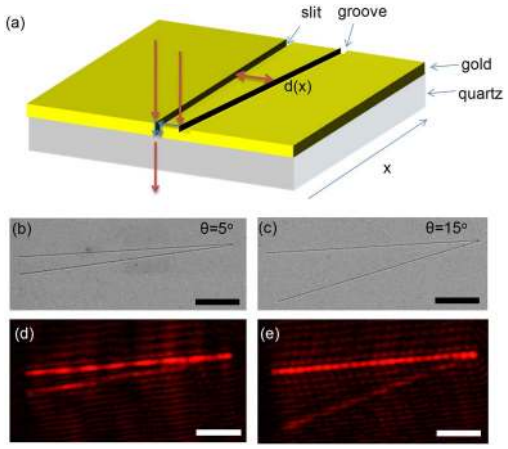

Fig. 1. (Color online) (a) Schematic representation of the plasmon interferometer. The interferometer is fabricated on a quartz substrate coated with 150 nm thick gold film; (b, c) Scanning electron microscope images of the fabricated plasmon interferometer with grove-slit angles of 5 and 15 degrees, respectively. The width of groove and slit are 200 nm and 100 nm, respectively; (d, e) Optical microscope images of the interference fringe pattern generated by the interference of SPPs excited by the groove-slit pair. The scale bars are 10 μm.

objective. The optical micrographs of high-contrast fringe patterns due to the interference of SPPs are shown in Fig. 1(d) and Fig. 1(e), for groove-slit angles of 5° and 15°, respectively. In contrast to the multispectral plasmon interferometers, the tilt angle allows us to obtain the interference pattern with monochromatic light. The SPPs interfere as they propagate through the slit. The plasmons generated by the groove accumulate a phase as they propagate across the separation distance between the groove and slit. Because the separation distance varies along the slit, a sinusoidal interference pattern is observed. We observed some level of transmission through the groove likely because of the inhomogeneous etching profile of the groove. The period of the interference pattern (Λ) can be written as $\Lambda = \lambda/n_{\text{eff}} \sin\theta$, where λ is the wavelength of the light source, n_{eff} is the effective index of SPPs, and θ is the tilt angle. The effective index can be written as $n_{eff} = [\varepsilon_d\varepsilon_m/(\varepsilon_d + \varepsilon_m)]^{1/2}$, where ε_m and ε_d are the dielectric constant of the metal and dielectric, respectively. The period for tilt angles of 5°, 10°, and 15° calculated for the goldwater interface are 5.08, 2.55, and 1.71 μm, respectively.

To test the performance of the sensor, we integrated the plasmon interferometer with a microfluidic device. The microfluidic device was fabricated using polydimethylsiloxane-based rapid prototyping [18]. The medium flowing inside the microchannel is deionized water, and the refractive index is controlled by varying the concentration of salt (NaCl). The interference pattern is imaged by a CCD camera. Figure 2(a) shows overlaid images of interference pattern obtained for various index of refraction between 1.34 to 1.37. There are 21 fringes in the length of 50 μm. We indexed the fringes starting from the intersection point of the groove and the slit. When we increased the refractive index of the liquid, we observed that the period of the interference pattern decreased and the fringes shifted spatially toward the intersection point. To guide the eye, we drew lines connecting the center of fringes in Fig. 2(a). The displacement of the fringes depends the total accumulated phase as SPPs move from the groove to the slit. This phase is a function of wavevector of SPP and the groove-slit separation distance as $\Delta\Phi(x) = k'_{\text{spp}}d(x)$. The fringe displacement increases linearly with the fringe number. The position of the first fringe (at the intersection point) stays constant owing to the small groove-slit separation distance. We measured the relative position of the fringes with respect to the first one. Figure 2(b) shows the intensity distribution of the first three fringes. Figure 2(c) shows the last four fringes on the interferometer. The fringe displacement increases linearly with the groove-slit separation distance. Figure 2(d) shows the fringe displacement for 1st, 14th, and 20th fringes as a function of index of refraction.

To understand the ultimate performance of the demonstrated plasmon interferometer, we have developed a numerical model to calculate the interference pattern and the detection sensitivity. As the surface is illuminated by collimated light, both groove and slit generate SPPs on the metal surface. The SPPs generated by the slit are transmitted through the metal, whereas the SPPs

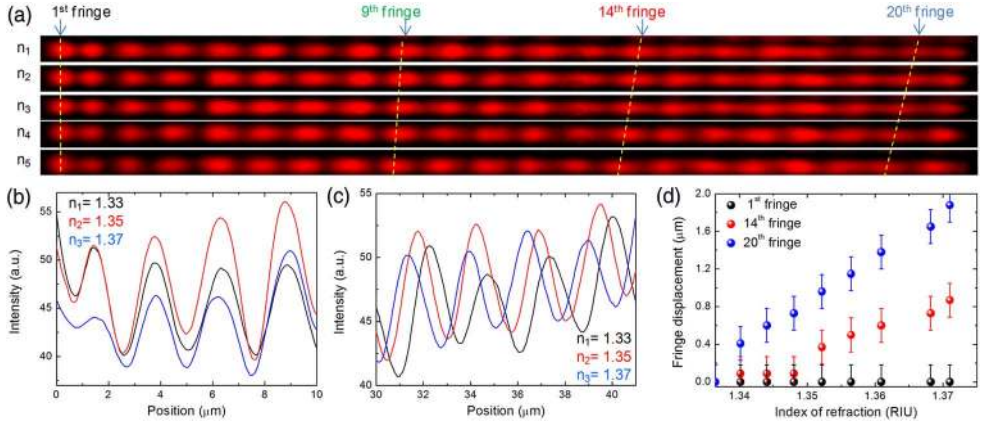

Fig. 2. (Color online) (a) Optical microscope images of the fringe pattern generated by plasmon interferometer with a tilting angle of 10°, integrated in a microfluidic device. The index of refraction of the medium is varied linearly between $n_1 = 1.34$ and $n_5 = 1.37$. The pattern has 21 fringes. The relative position of the fringes shifts as the index of refraction changes; (b, c) Spatial intensity distribution of the first and last four fringes. The relative positions of first fringes stay nearly constant; (d) Fringe displacement as a function of index of refraction. The slope of the curve provides the sensitivity of the sensor.

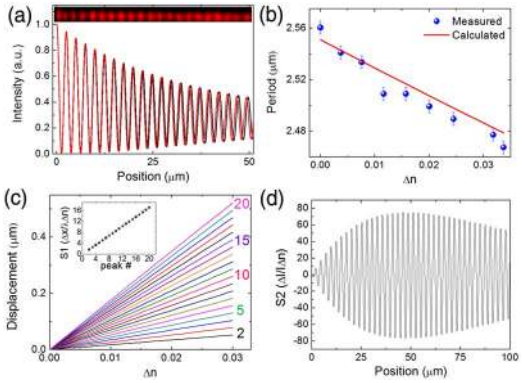

Fig. 3. (Color online) (a) Calculated interference fringes for two different indices of refraction ($n = 1.33$, dark curve; $n = 1.34$, light curve) generated by a plasmon interferometer with a length of 50 μm and a slit-groove angle of 10°. The inset shows the CCD image of the interference fringes; (b) Measured and calculated period of the fringe pattern as a function of change of index of refraction; (c) Normalized displacement of the fringes as a function of change of index of refraction. The inset shows the sensitivity as a function of fringe index; (d) Normalized intensity change along the slit position.

generated by the groove travel the slit-groove separation distance, $d(x)$ and then are transmitted to the other side of the metal. The presence of two phase-shifted electric fields at the slit position produces interference.

Total intensity of the transmitted light through the slit is written as [19,20] $I(x) = E_1(x)^2 + E_2(x)^2 + 2E_1E_2\cos(\Phi(x))$, where $E_1(x)$ and $E_2(x) \propto e^{-k''_{spp}d(x)}$ are the intensities of the transmitted light generated by slit and groove, respectively. The phase difference between the two electric fields is $\Phi(x) = k'_{spp}d(x) + \Phi_0$, where k'_{spp} and k''_{spp} are the real and imaginary part of the SP wavevector $k_{spp} = k'_{spp} + ik''_{spp}$. Φ_0 is an unknown constant phase shift that arises from the differences of the propagated distance in air and the coupling of SPs at the groove and the slit. The imaginary part of the wavevector defines the optical loss on the metal film. Figure 3(a) shows the calculated normalized intensity distribution along the interferometer with a slit-groove angle of 10°. The inset in Fig. 3(a) shows the recorded CCD image of the interference pattern. There is very good agreement between the observed and calculated fringe pattern. The contrast of the fringes decreases with increasing fringe number because of the optical loss of the metal. The period of the fringe pattern decreases with increasing index of refraction ($\Lambda = \lambda/n_{eff}\sin\theta$). Figure 3(b) shows the calculated (red line) and measured (scattered plot) period of the fringe pattern. An easy way to find the refractive index of the medium is to record the relative displacement of the fringes. Figure 3(c) shows the displacement of the fringes normalized by the period of the fringe pattern (Λ) as a function of change of index of refraction. The normalized displacement increases linearly with the fringe index. To quantify the sensitivity, we define two types of figure of merit; normalized displacement per refractive index, $S1 = \Delta x/\Lambda\Delta n$, and normalized intensity change per refractive index unit (RIU), $S2 = \Delta I/I\Delta n$. The inset in Fig. 3(c) shows the calculated displacement sensitivity $S1$ as a function of fringe index. Displacement sensitivity $S1$ of 17 RIU^{-1} can be obtained with the 21st fringe of a plasmon interferometer with a length of 50 μm. The calculated normalized intensity change per RIU, $S2$, is shown in Fig. 3(d) as a function of position along the slit. The sensitivity increases along the slit and reaches to a maximum value of 70 RIU^{-1} around 50 μm. For longer slit-groove distances sensitivity starts to decrease owing to the optical loss of the metal surface. With our imaging system, the minimum detectable refractive index change is around 3×10^{-4} RIU.

As a conclusion, we demonstrated a sensitive sensor based on a subwavelength plasmon interferometer. Oblique orientation of the slit-groove pair introduces a position-dependent phase difference, which generates repeating constructive and destructive fringes along the interferometer. Interrogation of the position and the intensity of the fringes provides a sensitive means for refractive index measurements. The small size of the sensor together with its ability to be integrated with microfluidic devices are the advantages of the presented sensor. The difficulty of the fabrication procedure using focused ion beam can be eliminated with nanofabrication techniques such as phase-shift lithography.

This work was supported by the Scientific and Technological Research Council of Turkey (TUBITAK) grant no. 110T304, Marie Curie International Reintegration Grant (IRG) no. 256458, Turkish Academy of Science (TUBA-Gebip).

References

1. D. Janasek, J. Franzke, and A. Manz, Nature **442**, 374 (2006).
2. P. Yager, T. Edwards, E. Fu, K. Helton, K. Nelson, M. R. Tam, and B. H. Weigl, Nature **442**, 412 (2006).
3. H. Craighead, Nature **442**, 387 (2006).
4. C. Genet and T. W. Ebbesen, Nature **445**, 39 (2007).
5. J. Homola, Anal. Bioanal. Chem. **377**, 528 (2003).
6. J. N. Anker, W. P. Hall, O. Lyandres, N. C. Shah, J. Zhao, and R. P. Van Duyne, Nat. Mater. **7**, 442 (2008).
7. A. V. Kabashin and P. I. Nikitin, Opt. Commun. **150**, 5 (1998).
8. M. Piliarik and J. Homola, Opt. Express **17**, 16505 (2009).
9. M. Okan, O. Balci, and C. Kocabas, Sens. Actuators B **160**, 670 (2011).
10. R. Slavik and J. Homola, Sens. Actuators B **123**, 10 (2007).
11. A. A. Yanik, M. Huang, A. Artar, T. Y. Chang, and H. Altug, Appl. Phys. Lett. **96**, 021101 (2010).
12. G. G. Nenninger, P. Tobiska, J. Homola, and S. S. Yee, Sens. Actuators B **74**, 145 (2001).
13. C. M. Jan, Y. H. Lee, and C. K. Lee, Plasmonics Biol. Med. **7**, 7577 (2010).
14. X. F. Wu, J. S. Zhang, J. J. Chen, C. L. Zhao, and Q. H. Gong, Opt. Lett. **34**, 392 (2009).
15. D. Braun and P. Fromherz, Phys. Rev. Lett. **81**, 5241 (1998).
16. M. J. Dicken, L. A. Sweatlock, D. Pacifici, H. J. Lezec, K. Bhattacharya, and H. A. Atwater, Nano Lett. **8**, 4048 (2008).
17. J. Feng, V. S. Siu, A. Roelke, V. Mehta, S. Y. Rhieu, G. T. R. Palmore, and D. Pacifici, Nano Lett. **12**, 602 (2012).
18. D. C. Duffy, J. C. McDonald, O. J. A. Schueller, and G. M. Whitesides, Anal. Chem. **70**, 4974 (1998).
19. V. V. Temnov, G. Armelles, U. Woggon, D. Guzatov, A. Cebollada, A. Garcia-Martin, J. M. Garcia-Martin, T. Thomay, A. Leitenstorfer, and R. Bratschitsch, Nat. Photon. **4**, 107 (2010).
20. V. V. Temnov, K. Nelson, G. Armelles, A. Cebollada, T. Thomay, A. Leitenstorfer, and R. Bratschitsch, Opt. Express **17**, 8423 (2009).